

Aerodynamic and Structural Design of MultiMW Wind Turbine Blades beyond 5MW

This article has been downloaded from IOPscience. Please scroll down to see the full text article.

2007 J. Phys.: Conf. Ser. 75 012002

(<http://iopscience.iop.org/1742-6596/75/1/012002>)

View [the table of contents for this issue](#), or go to the [journal homepage](#) for more

Download details:

IP Address: 38.107.179.211

The article was downloaded on 16/02/2012 at 01:32

Please note that [terms and conditions apply](#).

Aerodynamic and Structural Design of MultiMW Wind Turbine Blades beyond 5MW

B Hillmer¹, T Borstelmann¹, P A Schaffarczyk¹ and L Dannenberg¹

¹ CEWind, Mechanical Engineering Department, Kiel University of Applied Sciences

E-mail: benjamin.hillmer@fh-kiel.de

Abstract A unified approach was taken to the design of wind-turbine blades for multiMW machines up to 10 MW. Using input from standard existing machines, three baseline versions were designed. Then - after up-scaling - using the aero-elastic code FLEX5 a typical extreme load case was selected. As a result, weights seem to increase more than might be expected by an empirical law deduced from statistical data. However, some further investigations are needed, e. g. buckling and fatigue analyses. The authors regard the method developed here as a useful approach for pre-design investigation. One important aspect seems to be the need for high-quality GRPs, with admissible strength of more than 120 MPa.

1. Introduction

Wind turbine power is increasing steadily [1]. Offshore sites further than 10 km from the coast have to be planned with turbine sizes larger than the currently available 2 to 3 MW machines. Several 5-6 MW prototypes exist, having blades based on older technologies [2, 3] with lengths up to 61.5 m. Some of these have been tested offshore. Nevertheless new studies are under way [4] for which rated power output of 10 to 20 MW is the design goal, the most prominent of these being the DOWEC [5] and UPWIND-project [6].

This study focuses on the design of a rotor blade for an offshore wind turbine with an installed power exceeding 5 MW to 10 MW, using a traditional approach used in local industry.

We begin with an examination of a baseline 5MW blade mounted on a state-of-the-art multiMW wind-turbine. Typical wind loads, together with annual yield are simulated with the load case simulation software FLEX5 and stresses as well as weights are determined by a beam-element code. This results in up-scaled blades for 8 and 10 MW machines.

Results for annual yield and weights are reported by applying the procedure from the guidelines of Germanischer Lloyd Wind Energy (GL) [7].

2. Aerodynamic Design

2.1. Starting conditions

For the initial designs data such as the hub radius and the initial positioning of the various sections are adapted from existing turbines here. DU and NACA636xx airfoils were used.

Due to erosion problems the maximum tip speed is assumed to be to 80 m/s. The design tip speed ratio is deduced from the maximum wind speed operating at the optimum tip speed ratio and the maximum tip speed.

To avoid resonance problems the natural frequencies of the rotor blade are designed to be out of a $\pm 10\%$ deviation from the exciting rotor frequencies $1p$, $3p$ and $6p$.

2.2. Approach

The chord and twist distributions are calculated using a method of Wilson and Lissaman [8] which combines blade element momentum theory and a vortex theory for small perturbations. Prandtl's tip loss correction is applied. For a given radial section with known lift (c_l) and drag (c_d) coefficients, the local angle of attack θ which maximizes the power coefficient is given by

$$\theta_{opt} = \text{Max} \left[aF(a - aF) \left(\tan \theta - \frac{c_d}{c_l} \right) \right], \quad (1)$$

where F is the tip loss correction factor and a the axial induction factor. Three boundary conditions apply for the radius r of the section, the axial induction factor a and the radial induction factor a' . B denotes the number of blades, c the chord length and R the rotor radius.

$$r = R \frac{a}{a'} \frac{1 - aF}{1 - a} \tan \theta \quad (2)$$

$$a = \left\{ 2A + F - [F^2 + 4AF(1 - F)]^{\frac{1}{2}} \right\} \cdot (2(A + F^2))^{-1} \quad (3)$$

$$a' = \frac{Bcc_l}{2\pi r} \cdot \left(4F \cos \theta - \frac{Bcc_l}{2\pi r} \right)^{-1} \quad (4)$$

$$A = \frac{Bcc_l}{2\pi r} \cos \theta \cdot (4 \sin^2 \theta) \quad (5)$$

The set of equations (1) to (5) is solved by a double integration. The power coefficient is obtained by applying the following equation for a given tip speed ratio λ .

$$c_p = 8\lambda^{-2} R^{-3} \int aF(1 - aF) \left(\tan \theta - \frac{c_d}{c_l} \right) r^2 dr \quad (6)$$

2.3. Advanced aerodynamic methods

In 2.2 the basic inputs are the 2D polars usually deduced from measurements [9]. In this and related publications it was shown that the effect of Re on lift-to-drag ratio (L/D) is relatively small, so it was decided to use the same polars as for the 1-3 MW-class.

Three dimensional CFD is used for detailed investigation of parts of the wing close to the nose and tail. Most codes, however, do not have a transition prediction method, and transition determines the extent of laminar flow on a wing. A long run of laminar flow on a section is desirable to give high lift to drag ratios. In addition to the usual 2D e^N -method, which looks for instabilities of the (2D) laminar boundary layer due to Tollmien-Schlichting (TS) waves, in 3D flow, the so called Cross-Flow (CF) instabilities can occur [10]. Rotating flows clearly show these patterns even if fully attached, so this method is more accurate for investigating blade aerodynamics as it includes more physical phenomena.

Since the transition behavior of the boundary layer influences drag losses it is intended to estimate turbine power output with respect to the flow regime.

3. Load case calculation

3.1. Simulation Model

The load case calculations are performed with the widely-used FLEX5 software which is based on the blade element momentum theory in the time domain.

The blade data is determined by the aerodynamic and structural design. The initial stiffness and mass distributions are estimated from data for existing wind turbines. A power curve for the inverter has been adapted for each blade design. Data for other components of the turbine are taken from an existing smaller turbine that has been scaled up. Parameters for other components have been changed only in order to avoid possible resonance problems.

3.2. Load Cases and Evaluation

The turbine is simulated with external conditions for type class I according to IEC 61400-1 (ed.2) and the guidelines of the GL respectively [11]. For an offshore site the category for lower turbulence intensity values (category C) has been selected. Wave loads are not considered as they are highly dependent on the foundation and tower which would be different for an up-scaled case.

Apart from external conditions, simulations depend on turbine-specific parameters. The loads due to starting and stopping depend on the operation system. Gusts and operation faults lead to loads dependent on the control system. In order to focus on the blade design only two groups of load cases are considered, 24 load cases from 2 to 25 m/s wind speed at operating conditions (DLC1.1) and one load case at parking condition with the extreme wind speed model (DLC6.1).

Extreme loads are obtained by selecting minimum and maximum values of the simulated time series at two specific radial stations. Preliminary calculations showed critical areas at the blade root and at $0.3 \times$ blade radius. For structural analysis these values are used together with appropriate time equivalent loads. Fatigue loads have not yet been investigated.

The energy yield is again calculated by simulation of operating conditions according to DLC1.1 but with reduced turbulence intensities and reduced oblique inflow angles. The calculated power performances are weighted with a Weibull wind distribution. The parameters $A=11.2$ m/s and $k=2.26$ are taken from two years of measurements on the research platform FINO 1 (Jan 04 to Dec 2005) [12].

4. Structural Design

4.1. Approach

This calculation uses a right-handed coordinate system with the z-axis along the pitch-axis and the origin located at the center of the blade root, according to the chord coordinate system of GL Wind [7].

The scaling law is applied using the same tip-speed-ratio, airfoil section, number of blades, material and geometric similarity.

This leads to following formulas [13] for both values of the total gravity force G and the aerodynamic force A with respect to the radii R :

$$\frac{G_2}{G_1} = \left(\frac{R_2}{R_1} \right)^3, \quad \frac{A_2}{A_1} = \left(\frac{R_2}{R_1} \right)^2. \quad (7)$$

Bending stresses σ_A of aerodynamic forces are scaled with the power of 0, whereas the bending stresses σ_G due to gravity are scaled with the power of 1:

$$\frac{\sigma_{G2}}{\sigma_{G1}} = \left(\frac{R_2}{R_1} \right)^1, \quad \frac{\sigma_{A2}}{\sigma_{A1}} = \left(\frac{R_2}{R_1} \right)^0. \quad (8)$$

It is obvious that with growing blade length the blade mass becomes the critical factor for the maximum size of the blade.

For each cross-section defined in the structural model for the blade, the global center of area, the geometrical moment of inertia, the section modulus and the first order moment are determined.

Discrete forces and moments for the 21 sections are passed directly from the Flex Program. A total equivalent distributed load is created from the FLEX data. The overall bending moments and shear forces for the airfoil are determined by integrating this distributed load. It should be noted that for the purposes of the calculation all forces and moments are resolved along the appropriate axes.

According to GL the maximum shear stress for GRP shall not exceed $\tau_{\max} = 7$ MPa. The authors have specified the maximum bending stress to be $\sigma_{\max} = 120$ MPa.

4.2. Calculation

The basis of this calculation is a simplified beam theory model. Each cross-section is therefore divided into three basic geometrical shapes, a rectangle representing the box spar, a half ellipsoid and a triangle representing the leading and trailing edges respectively. To simplify the calculations a symmetrical cross section is assumed. The spar is linearly tapered from the blade root to the tip. All applied loads are transformed along the appropriate axes to find the appropriate stresses along these axes. Then the stress formulas become

$$\sigma(x, y, z) = -\frac{M_x(z)}{I_x(z)} \cdot y + \frac{M_y(z)}{I_y(z)} \cdot x \quad , \quad (8)$$

$$\tau(s, z) = -\frac{Q_x(z) \cdot S_y(s, z)}{I_y(z) \cdot t(s, z)} - \frac{Q_y(z) \cdot S_x(s, z)}{I_x(z) \cdot t(s, z)} \quad . \quad (9)$$

The stress σ is dependent on the bending moments M , the moments of inertia I , and the various local distances. The shear force Q , the first order area-moment S and the moment of inertia give the shear flux. The shear-stress τ is the quotient of the shear flux and thickness t .

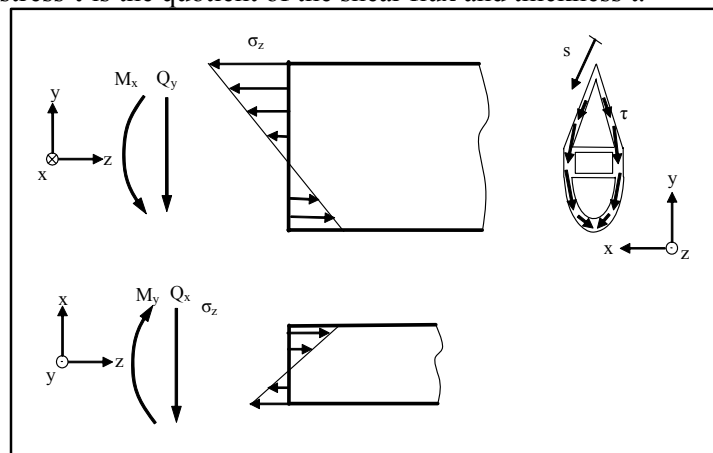


Figure 1. Bending stress σ and shear stress τ are related to the bending moments M and shear forces Q .

Bredt's formulas are used for the calculation of the torsional shear stress. For simplicity, the airfoil is considered to be a thin-walled single-celled closed frame. The lowest natural frequencies are calculated using the vibration theory of beams.

4.3. Optimization

At this point in the optimization process, the material thickness of the airfoil shell, the web and the flange of each cross section is altered iteratively using the extreme values of all load cases. This is assumed to assure sufficient strength for minimum weight.

The resulting blade design is used for a load case calculation. Stresses and natural frequencies are analyzed for these extreme loads. The cycle is repeated until stiffness and mass distributions converge.

5. Results

The first aerodynamic design results in an unrealistic rotor blade shape with high chord values for the inner sections and discontinuities at defining airfoil sections. Version A is obtained from smoothed twist and chord distributions (figure 2). This new shape gives a smaller blade area. As a consequence the optimum tip speed ratio is increased (figure 3).

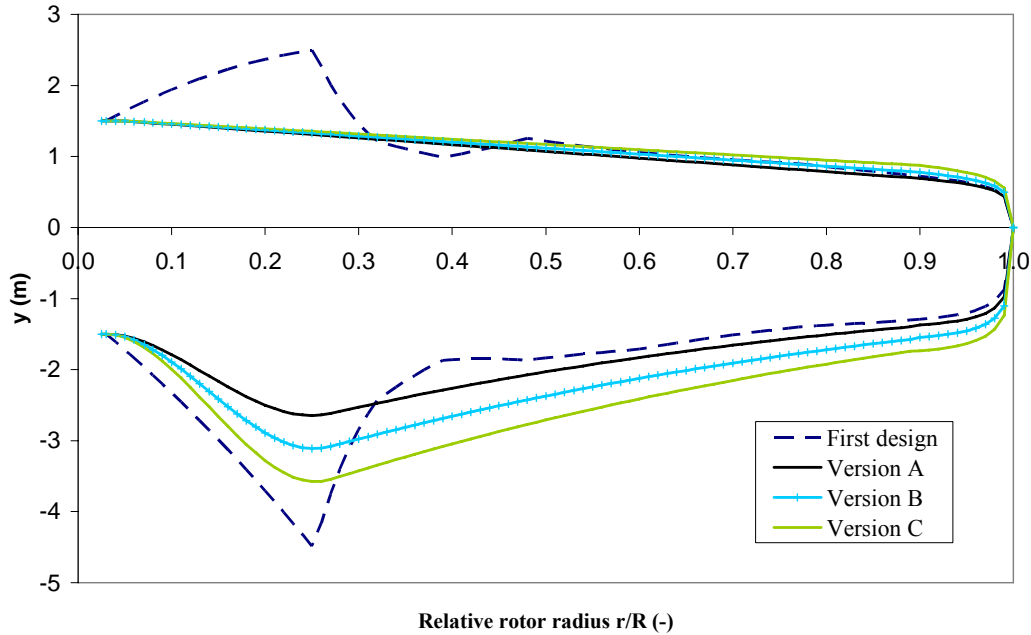


Figure 2. Rotor blade shape for the different versions.

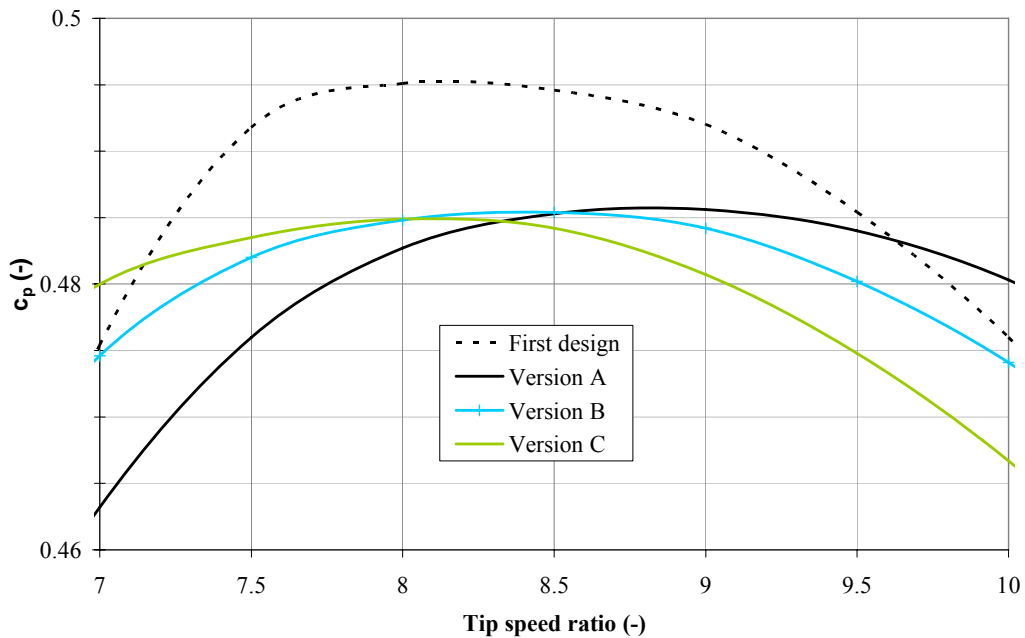


Figure 3. Power coefficient c_p and tip speed ratio for different versions.

As the turbine will operate with a limited tip speed ratio, two versions are created by modifying the chord length. Hence, versions B and C of the rotor blade show increased chord length and decreased optimum tip speed ratios.

Table 1. Versions of the 5MW, 116m rotor blade

	Version A	Version B	Version C
Optimum tip speed ratio	8.8	8.4	8.0
Mass (t)	20.6	20.7	16.3
Natural frequency flapwise (Hz)	0.96	0.89	1.14
Difference to 6p excitation (%)	-27	-33	-13
Natural frequency edgewise (Hz)	1.59	1.44	1.78
Difference to 6p excitation (%)	+21	+10	+35
Annual energy yield (10 ⁶ kWh)	22.1	23.1	23.7
Maximum tip displacement (m)	5.4	5.7	3.5

The limitation of the edgewise frequency led to a relatively heavy Version B. Its weight could possibly be reduced by a more detailed structural design. A small blade area results in lower aerodynamic loads while idling in extreme wind conditions. On the other hand small chord lengths require larger wall thicknesses of the inner structure. The optimal compromise has not been determined in this study so far. Version B alone was to give scaled to a rotor blade of 73m and 82m radius and optimized weight.

Table 2. Comparison of scaled rotor blades

Rotor blade radius	58m	73m (scaled)	82m (scaled)
	(Version B)		
Turbine power (MW)	5.0	8.0	10.0
Natural frequency flapwise (Hz)	0.89	0.75	0.67
Difference to 6p excitation (%)	-33	-29	-28
Natural frequency edgewise (Hz)	1.44	1.16	1.03
Difference to 6p excitation (%)	+10	+11	+10
Mass (t)	20.7	40.9	54.7
Maximum tip displacement (m)	5.7	6.4	7.5

Figure 4 shows the blade mass in comparison to some existing rotor blades [14]. Additionally, an empirical power law with an exponent of 1.9 is deduced.

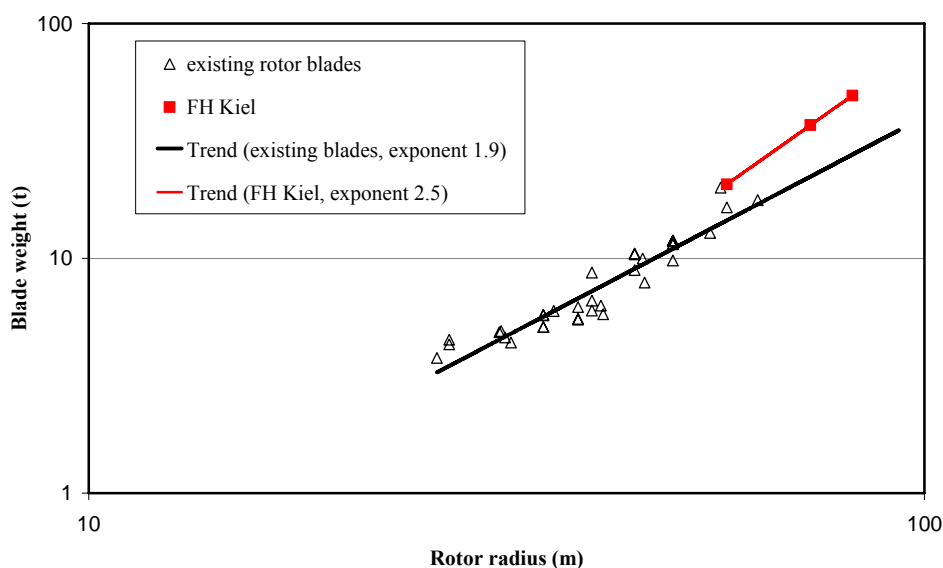


Figure 4. Comparison of rotor blade weights for different rotor radii

The 58 m blade is close to the empirical trend line. The masses of the 73 m and 82 m rotor blades increase with an exponent of 2.5. Due to slight modifications in the mass distributions, this is less than the theoretical value of 3.

On the basis of these theoretical scaling laws, geometrically similar scaling results in a linear growth of the bending stresses due to gravity whereas the stresses due to aerodynamic and centrifugal forces will remain constant. The calculated gravity-induced flapwise bending stresses normalized by the stress limit σ_{\max} are shown in figure 5. These ratios have been calculated for a horizontal rotor blade with a pitch of 90° . These values remain below the theoretical linear increase with respect to the radius (7% for 73m, and 9% for 82m radius). This is due to slight modifications of the mass distribution in order to minimize the total blade mass.

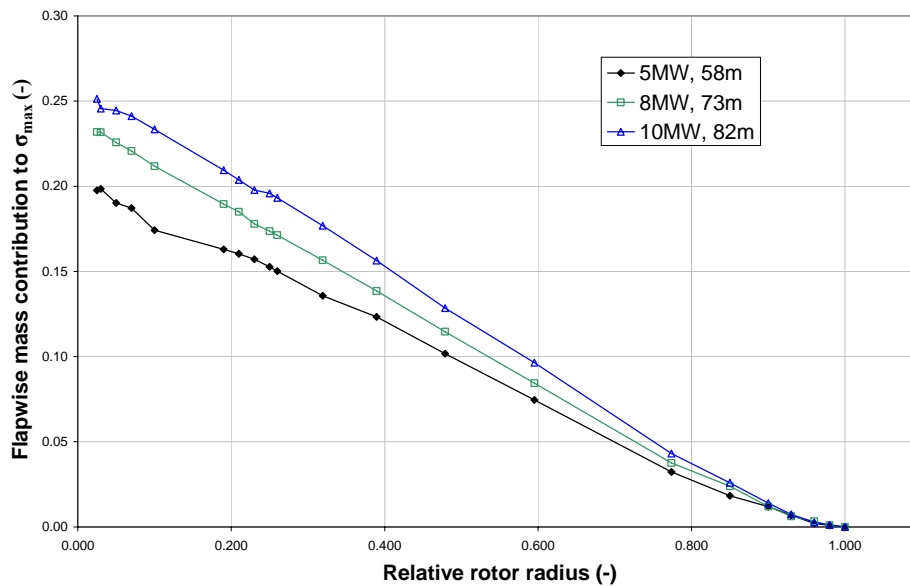


Figure 5. Ratio of flapwise bending stresses due to gravity and stress limit σ_{\max} plotted against relative rotor radius for different rotor blade sizes

Gravity induced edgewise stresses have been calculated for a horizontal rotor blade with a pitch of 0° . These values range from 0.28 to 0.35 at the blade root. Assuming a linear growth, gravity-induced stresses would exceed the aerodynamic stresses at the blade root only for rotor radii beyond approximately 100 m.

6. Conclusions

In spite of some structurally simplified model the weight for the 5MW rotor blade is a fairly good estimation of existing rotor blades. The linear growth in weight with respect to the radius could be slightly reduced by a modification of the mass distributions.

The domination of gravity-induced stresses is expected at the blade root for rotor radii beyond approximately 100 m. For larger rotor blades another structural design and materials with higher admissible strength would be needed.

7. Future Work

So far, the airfoil section has been treated as a thin-walled single-celled frame. It became obvious that in the course of this study that the sections should be treated as multi-cellular objects. The currently numeric analysis serves mainly for the preliminary design of the model. For a more accurate analysis the generation of an FE model is indispensable. This FE model is the next step in the study and will be used to determine the buckling behavior of the whole airfoil and to give an improved analysis of natural frequencies.

Together with an advanced load evaluation procedure these calculations will form the basis for the fatigue calculations necessary for further investigations of large rotor blades.

Furthermore, a detailed elaboration of the glass-fiber-reinforced laminate composition will be performed as so far neither the laminate nor a foam inlay have been considered during strength and weight calculations. The final task is to further develop the design and construction of the airfoil-hub fairing and to integrate this into the overall design process.

References

- [1] Harrison R, Hau E and Snel H: "Large Wind Turbines", John Wiley & Sons, Chicester, 2000
- [2] Jackson K H, Zuteck M D, van Dam C P, Standish K J and Berry D, *Innovative Design Approaches for Large Wind Turbine Blades*, WIND Energy, **8**, 141-171 (2005)
- [3] TPI Composites, *Innovative Design Approaches for Large Wind Turbine Blades*, SAND2003-0723, Sandia National Laboratories, Albuquerque, NM, (2003)
- [4] Jonkman, J., private Communication
- [5] Jensen P H, UpWind workshop, EWEC 2007, Milan, Italy, private Communication
- [6] Kooijman, H.T.J.T, Lindenburg, C; Winkelaar, D. and Van der Hooft, E.L, DOWEC 6 MW Pre-Design, DOWEC-F1W2-HJK-01-46/9, Sepz. 2003
- [7] Germanischer Lloyd, Rules and Guidelines, IV - Industrial Services, Part 1 - Guideline for the Certification of Offshore Wind Turbines, Edition 2005
- [8] de Vries O; "Fluid Dynamic Aspects of Wind Energy Conversion"; ISBN 92-835-1326-6, AGARDograph No. 243, 1979, p. 4-13
- [9] Freudenreich K, Kaiser K, Schaffarczyk A P, Winkler H and Stahl B, Reynolds Number and Roughness Effects on Thick Airfoils for Wind Turbines, Wind Engineering, **28**, 529-546, (2004)
- [10] Krumbein A, Automatic Transition Prediction and Application to 3D Wing Configurations, AIAA-2006-0914 (2006)
- [11] IEC 61400-1, Ed. 2, Wind Turbine Generator Systems - Part 1: Safety Requirements, 1999
Germanischer Lloyd, Rules and Guidelines, IV - Industrial Servicews, Part 1 - Guideline for the Certification of Wind Turbines, Edition 2003 with Supplement 2005
- [12] Neumann T.; Riedel V.; "FINO 1 Platform: Udate of the Offshore Wind Statistics"; DEWI Wilhelmshafen, DEWI-Magazin Nr. **28**, 28.Feb. 2006, p. 60
- [13] Gasch, R; Twele, J; Power Plants: "Fundamentals, Design, Construction and Operation", Chap. 8, James & James, Oct 2002, ISBN-10: 1902916379, ISBN-13: 978-1902916378
- [14] LM Glasfiber A/S, Rolles Mollevej 1, DK-6640 Lunderskov, private communication
EUROS Entwicklungsgesellschaft für Windkraftanlagen, Falkenberger Str. 146A/B, 13088 Berlin, Germany, private communication